Pinning Efficiency of One-Dimensional Artificial Pinning Centers in $YBa_2Cu_3O_{7-x}$ Thin Films

Judy Wu, Bibek Gautam, Mary Ann Sebastian, Victor Ogunjimi, Shikhar Misra, Jijie Huang, Javier Baca, Joseph Prestigiacomo, Timothy Haugan, Haiyan Wang, and Mike Osofsky

(Invited Paper)

***Abstract*—$BaZrO_3$ (BZO) and $BaHfO_3$ (BHO) form the comparable diameter ∼5–6 nm of one-dimensional artificial pinning centers (1-D APCs) in $YBa_2Cu_3O_{7-x}$ (YBCO) film. However, the lattice mismatch ∼7.7% at the BZO/YBCO interface is slightly higher than ∼7.1% at the BHO/YBCO interface. This leads to a much reduced interface dislocation density, and coherent interface at the BHO/YBCO film that has found a critical effect on the pinning efficiency of the 1-D APCs. This paper thus presents a quantitative comparison of pinning efficiency of single doped 4.0 vol.% BZO/BHO (SD) and double doped 4.0 vol.% BZO(BHO) + 3.0 vol.% Y_2O_3 doped (DD) YBCO films. A significantly higher pinning efficiency in terms of a maximum pinning force density $F_{p,max}$ ∼182 GN/m^3 at $H_{max} > 9.0$ T for BHO SD film may be due to coherent interface. This is about 2.5 times higher than that of its BZO SD counterparts at 65 K. In addition, the ratio of H_{max} and H^*(accommodation field determined from the areal density of the 1-D APCs using TEM) is calculated about 0.74 and 0.53 for BHO SD and BZO SD films, respectively. This value is about 0.65 and 0.82 for BHO DD and BZO DD films, respectively at 65 K.**

***Index Terms*—1D artificial pinning centers, APCs of mixed morphologies, coherent interface, pinning efficiency, YBCO nanocomposite film.**

I. Introduction

In THE past decade or so, the enhancement of the vortex pinning in high temperature superconductors (HTSs) such as rare earth compounds Re(= Y,Sm,Gd)$Ba_2Cu_3O_7$ (ReBCO) has been investigated by many groups through self-assembly of nanoscale artificial pinning centers (APCs) of the desired dimensions and morphology in HTSs [1]–[4]. Many APC materials have been reported including $BaZrO_3$ (BZO), $BaSnO_3$ (BSO), $BaHfO_3$(BHO), YBa_2(Nb/Ta)O_6, Y/Gd/Sm)$Ba_2Cu_3O_{7-x}$ and Y_2O_3 [4]–[10]. The processes for self-assembly of APCs in ReBCO include pulse laser deposition (PLD), metal organic chemical vapor deposition, solution method [11]–[15]. Considering the anisotropy of the pinning due to layered structure of the HTS materials, one dimensional (1D) APCs aligned in the *c*-axis have received particular attention since they have shown to provide strong correlated pinning and hence enhance the critical current density J_c in magnetic field (H) at H//c-axis. Consequently, a broad peak of J_c centered at H//c-axis with respect to the orientation of the magnetic field (typically defined by angle θ with $\theta = 0$ at H//c-axis and $\theta = 90$ degree at H//ab-plane) can be observed, resulting in reduced the J_c-anisotropy in magnetic fields.

In ReBCO films and coated conductors, the *c*-axis aligned 1D APCs of BZO [16], BSO [11], and BHO [17], [18] have been studied intensively. While all these 1D APCs have shown correlated pinning at H//c-axis, a fundamental question arises on what determines the pinning efficiency of an individual 1D APC quantitatively? In order to shed light on this important question, this work investigates the pinning efficiency of BZO and BHO 1D APCs in YBCO films. The BZO and BHO 1D APCs have comparable diameters of 5–6 nm, allowing minimization of the complication of the size effect on the pinning efficiency. Moreover, the lattice mismatch at the BZO/YBCO interface is ∼7.7%, which is slightly higher than that at the BHO/YBCO interface of ∼7.1%. This difference provides an excellent opportunity to investigate the effect of the 1D APC/YBCO interface on the pinning efficiency of these 1D APCs.

Specifically, the pinning efficiency of 1D APCs can be evaluated quantitatively from the transport measurement of critical current density $J_c(H)$ at H//c-axis and from which the pinning force density $\boldsymbol{F}_p = \boldsymbol{J}_c \times \boldsymbol{H}$ can be derived. By choosing 4 vol.% BZO and BHO single-doped YBCO, the comparison of the $F_p(H)$ curves at H//c-axis and 65–77 K and the microstructures of the APC/YBCO interfaces would allow correlation of the pinning efficiency and the interface microstructure. Considering the pinning efficiency of a 1D APC may extend to a

Manuscript received October 29, 2018; accepted January 23, 2019. Date of publication January 28, 2019; date of current version February 6, 2019. This work was supported in part by National Science Foundation under Contracts NSF-DMR-1508494 and NSF-ECCS-1809293/1809284, in part by the Air Force Research Laboratory Aerospace Systems Directorate, in part by the Air Force Office of Scientific Research, and in part by the U.S. National Science Foundation (DMR-1565822) for TEM characterization. *(Corresponding authors: Judy Wu and Bibek Gautam.)*

J. Wu, B. Gautam, V. Ogunjimi, and J. Baca are with the Department of Physics and Astronomy, University of Kansas, Lawrence, KS 66045 USA (e-mail: jwu@ku.edu; gautbibe@ku.edu; victorogujimi@ku.edu; f.javier.baca@gmail.com).

M. A. Sebastian and T. Haugan are with the U.S. Air Force Research Laboratory, Propulsion Directorate, Wright-Patterson AFB, Dayton, OH 45433 USA (e-mail: mary_ann.sebastian.1.ctr@us.af.mil; timothy.haugan@us.af.mil).

S. Misra, J. Huang, and H. Wang are with the School of the Material Engineering Purdue University, West Lafayette, IN 47907 USA (e-mail: misra4@purdue.edu; haun1027@purdue.edu; hwang00@purdue.edu).

J. Prestigiacomo and M. Osofsky are with the U.S. Naval Research Laboratory, Washington, DC 20375 USA (e-mail: joseph.prestigiacomo@nrl.navy.mil; michael.osofsky@nrl.navy.mil).

Color versions of one or more of the figures in this paper are available online at http://ieeexplore.ieee.org.

Digital Object Identifier 10.1109/TASC.2019.2895739

small angular range of θ around $\theta = 0$ (H//c-axis), the angular range of the 1D APC pinning efficiency is also investigated. In addition to BZO or BHO single-doped YBCO samples, two double-doped samples were also included in this study assuming a secondary APC of 3 vol.% of Y_2O_3 modifies the 4 vol.% BZO or BHO 1D APC/YBCO interfaces and therefore affects their pinning efficiency. The enhanced $J_c(H//c)$ with significantly higher $F_{p,max}$ about 2.5 times and H_{max}/H^* (H_{max} is at which the $F_{p,max}$ is observed and H^* is an accommodation field calculated from interspace distance of APCs in TEM images) about 1.5 times higher for the BHO/YBCO SD film is observed compared to its BZO/YBCO counterparts. Considering $F_{p,max}$ and H_{max}/H^* are quantitative expression of pinning efficiency, this difference of pinning efficiency could be due to coherent BHO APC/YBCO interface in BHO SD film in contrast to semi-coherent BZO APC/YBCO interface in BZO SD film [19]. The pinning efficiency of the 1D APCs is extended to about 22° in both BZO/YBCO SD and DD films.

II. Experiment

BZO(BHO)/YBCO single and double doped nanocomposite thin films were fabricated using pulsed laser deposition (PLD) from targets with 4.0 vol.%, BZO(BHO) and 4.0 vol.%, BZO(BHO)+ 3.0 vol.% of Y_2O_3 concentration respectively. These films will be regarded as 4% SD and 4% DD for BZO (BHO)/YBCO and [BZO (BHO) + Y_2O_3]/YBCO films respectively in the following. In an analogous way, the SD and DD samples will be regarded as BZO (BHO)-SD, and DD nanocomposite films for simplicity. The BZO (BHO) - SD and DD films were deposited on (100) $SrTiO_3$ (STO) single crystal substrates at the substrate temperature of 825 °C (810 °C) and for in 300 mTorr oxygen (O_2) pressure. After deposition, the films were annealed for about 30 minutes at 500 °C in one atmosphere O_2 pressure. Films thicknesses were measured using K-16 Tencor profilometer in the range of 140 nm–160 nm. Films were patterned using standard photolithography to obtain microbridges width of ~20 and 40 μm, and length of ~500 μm for the electric transport measurement. J_c was calculated by applying standard 1 μV/cm criterion. A Quantum Design Evercool II Physical Property Measurement System (PPMS) was used for measuring the transport $J_c(T, H, \theta)$ as function of temperature T (65 K-77 K), magnetic field H (0.0-9.0 T), and the angle θ between the c-axis and H. The field H was maintained in the plane perpendicular to the current. Lattice parameters were determined by X-ray diffraction (XRD) analysis utilizing the Bruker D8 Discover diffractometer [15]. The microstructure and morphology of the APCs nanostructures of the films were analyzed using Transmission Electron Microscopy images taken from the FEI Tecnai F20 analytical microscope.

III. Results and Discussion

Figures 1(a)-(b) and 1(c)-(d) compare the XRD θ-2θ spectra for the BZO (BHO) SD and DD nanocomposite films respectively. The clearly visible YBCO (001) peaks illustrate the highly crystalline c-axis orientation normal to the surface of the films. Some of the minor peaks are index as the BZO (BHO) and Y_2O_3 peaks. In addition, YBa_2ZrO_6 peak around 40 degrees in

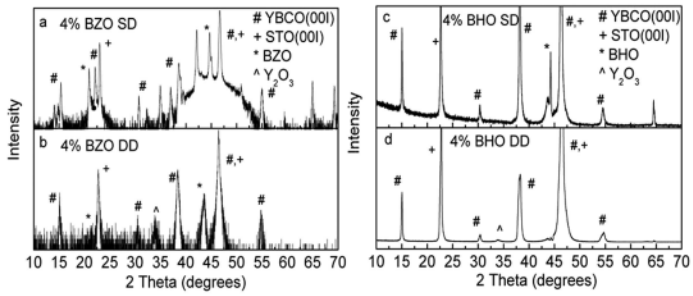

Fig. 1. (a)-(b) XRD θ-2θ spectra for the 4% BZO SD and DD, and (c)-(d) 4% BHO SD and DD nanocomposite films on STO substrates respectively. Indices follow the same for each set of figures.

TABLE I
General Parameters C-Axis Lattice Constant, FWHM of YBCO (005) Peaks, Critical Temperature T_c, 1D APC Diameter and Inter 1D APC Spacing Measured From Center to Center, Accommodation Field ($H^* = \phi_o/D^2$), Maximum Pinning Force Density ($F_{p,max}$) and Matching Field (H_{max}) at 77 K and 65 K for the BZO (BHO) SD and DD Films

Sample ID	c-axis lattice constant (Å)	FWHM of YBCO (005) peak	T_c (K)	1D APC Diameter (nm)	1D APC Spacing (D) (nm)	H^* (T)	H//c-axis and at 77 K		H//c-axis and at 65 K	
							$F_{p,max}$ (GN/m³)	H_{max} (T)	$F_{p,max}$ (GN/m³)	H_{max} (T)
4 vol.% BHO SD	11.76	0.51	85.84	4.8	13.0	12.2	22.8	7.5	182	>9.0
4 vol.% BZO SD	11.71	0.35	87.48	5.8	15.0	9.2	13.33	4.0	72.37	5.0
4 vol.% BHO DD	11.75	0.75	86.6	4.6	13.0	12.2	7.36	4.0	67.72	7.5
4 vol.% BZO DD	11.72	0.82	87.69	5.7	15.0	9.2	3.33	5.5	49.49	8.0

BZO SD film indicates the induction of Zr in YBCO matrix while such a peak is not visible in BZO DD and BHO films. It means Y_2O_3 may suppress the Zr diffusion in the BZO DD film and Hf diffusion in YBCO matrix is not as easy as Zr diffusion. The c- axis lattice constant of the SD and DD films are almost constant individually for BZO and BHO films (Table I) while slightly higher strained c-axis lattice (~11.75–11.76 Å) for BHO films is observed compared to c-axis lattice (~11.71–11.71 Å) for BZO films. It indicates that the coherent APC/YBCO interface is maintained for BHO films through strained c-axis lattice compared to strain released through defects and dislocations in BZO films reducing coherency of APC/YBCO interface. The larger values of full width at half maximum (FWHM) of YBCO (005) peaks measured from rocking curves (not shown in Figure) for DD films, compared to FWHM of SD films (Table I) is an indication of lattice distortion of the DD films due to additional Y_2O_3 nanoparticles. In fact, the dislocation and defects at the APC/YBCO interface leads to c-axis lattice distortion and increased FWHM in DD films. The increment of FWHM in BHO DD film (~0.25) is about half of the increment of BZO DD film (~0.5) compared to their SD counterparts indicates the higher distortion of lattice by additional Y_2O_3 in BZO films in compared to BHO films. The higher of T_c values for both BZO (BHO) DD films compared to SD films counterparts indicates the reduction of strain field overlap by addition of secondary dopant Y_2O_3 in DD films. However, such increment is higher in BHO films from 85.84 K to 86.60 K than that of BZO films from 87.48 K to 87.69 K (Table I).

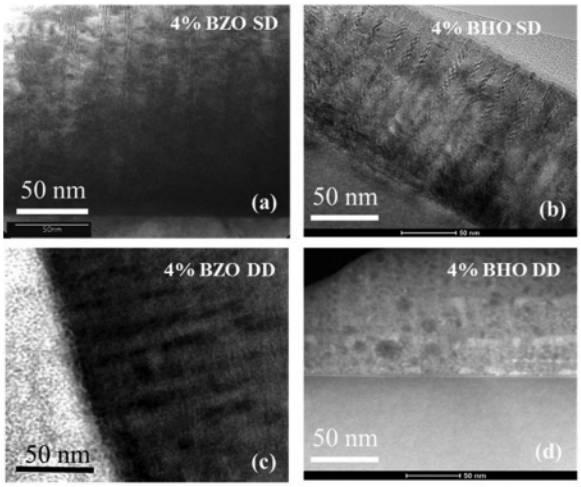

Fig. 2. Cross sectional TEM image of YBCO nanocomposite films doped with (a) and (b) 4 vol.% BZO and 4 vol.% BZO plus 3 vol.% Y_2O_3 (c) and (d) 4 vol.% BHO and 4 vol.% BHO plus 3 vol.% Y_2O_3 films respectively.

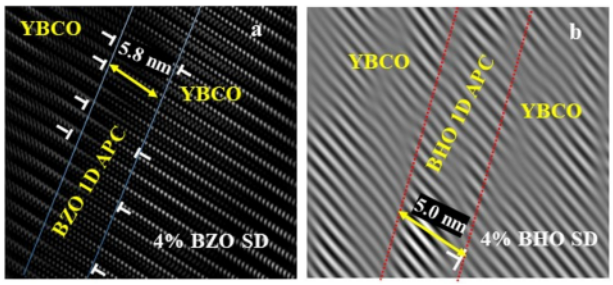

Fig. 3. Fast Fourier filtered images of (a) 4% BZO SD and (b) 4% BHO SD films.

To understand the microstructures transmission electron microscopy (TEM) images are taken for SD films (top row) and DD films (bottom row) as shown in Figures 2(a)-(d). Cross sectional TEM images of both SD films show long 1D-APCs through the thickness of the films which are mainly responsible for strong correlated pinning. The diameter of BZO 1D APC is found to be 6.0 nm while that of BHO 1D APCs is about 5.0 nm separated by ~15 nm and 13 nm respectively. Considering the independent growth of BZO (BHO) and Y_2O_3 phase, similar diameter and inter APCs distances are considered in DD films. In addition, few Y_2O_3 nanoparticles considered as 3D APCs are visible in both BZO and BHO DD films. BHO DD film shows more mixed (1D+3D) APCs morphology but with short and segmented *c*-axis aligned 1D APCs and 2D APCs aligned along *ab*-plane while 2D APCs are not clearly seen in BZO DD film. Based on the TEM observation, it can be claimed that DD films have mixed APCs morphology while SD films do not have such mixed APCs morphology.

Figures 3(a)-(b) shows the fast Fourier filtered images of BZO SD and BHO SD films showing a difference of BZO APC/YBCO and BHO APC/YBCO interface and the ways of interfacial strain relax. A semi-coherent BZO APC/YBCO interface with less strained *c*-axis lattice due to dislocations and defects for BZO film is observed compared to coherent APC/YBCO interface is expected for BHO film with slightly higher strained *c*-axis lattice but almost constant for SD and

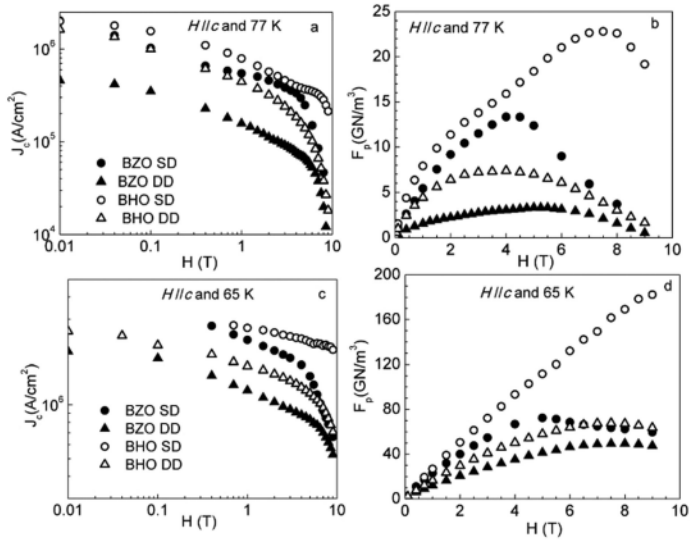

Fig. 4. J_c(H) and $F_p(H)$ curves measured on 4% BZO and 4% BZO plus 3% Y_2O_3 (solid), and 4% BHO only, and 4% BZO (BHO) plus 3% Y_2O_3 (open) doped YBCO nanocomposite films at $\theta \sim 0^o$ ($H//c$-axis) (a) and (b) at 77 K, (c) and (d) at 65 K respectively. Symbols are SD (circle) and DD (triangle) follow the same for all figures.

DD films. In BZO/YBCO, strain is released through large interfacial defects while at BHO/YBCO it does through large plane buckling as indicated in Figures 3(a)-(b). The difference of APC/YBCO interface in fact influences the pinning efficiency of the 1D APCs as explained in the following paragraphs.

Figures 4(a)-(b) and 4(c)-(d) compare the $J_c(H)$ and $F_p(H)$ curves for the BZO SD and DD (black) and BHO SD and DD (blue) nanocomposite films of 4 vol.% BZO (BHO) concentrations at H//c-axis, and at 77 K and 65 K respectively. Similar trend but the higher $J_c(H)$ curves for SD films compared to DD films at 77 K and 65 K shows the significance of the strong correlated pinning of 1D-APCs in both SD films compared to their DD counterparts respectively. However, comparing with BZO and BHO doping along with Y_2O_3, the higher $J_c(H)$ curves for both BHO SD and DD films is an indication of the strong correlated pinning as well as coherent interface of BHO APCs/YBCO compared to semi-coherent interface of their BZO/YBCO counterparts both at 77 K and 65 K. In fact, extra Y_2O_3 adds more compressive strain to the YBCO lattice of the BZO DD film compared to the BHO DD film, and hence the comparatively shorter *c*-axis lattice constant is observed in former compared to latter. On the other hand, the overall low $J_c(H)$ values of the DD films compared to SD films for both doping seem consistent with microstructure of TEM images of short *c*-axis aligned 1D APCs and mixed APCs in the DD films (Figure 2(c)-(d)). Also, the smaller $\Delta T_c \sim 0.21$K for BZO films compared $\Delta T_c \sim 0.76$ K BHO films with addition of Y_2O_3 indicates the reduction of strain field overlap is more in BHO films through mixed APCs. At 65 K, the highest $J_c(H)$ values at the field up to 9.0 T for BHO SD film indicate there could be a coherent BHO APCs/YBCO interface which is consistent with the almost the same *c*-axis lattice constant.

The $F(H)$ curves follow the similar trend as of $J_c(H)$ curves for both SD and DD films at both 77 K and 65 K respectively. The higher $F_{p,max} \sim 23$ GN/m^3 and ~182 GN/m^3 for BHO SD

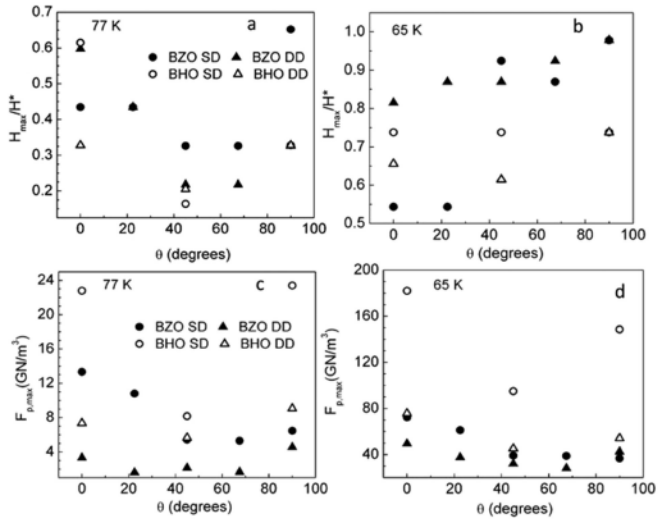

Fig. 5. Temperature dependence of (a) H_{max}/H^* ratio; and (b) $F_{p,max}$ for the SD (circle) and DD (triangle) of BZO (solid) and BHO (open) nanocomposite films at 77 K and 65 K respectively. The arrow indicates the value would go higher but instrument limitation applies.

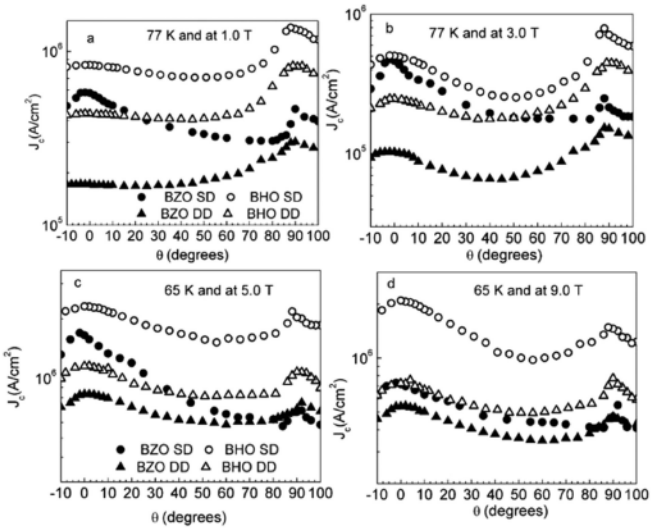

Fig. 6. Angular dependence of J_c measured on 4% BZO and 4% BZO plus 3% Y_2O_3 (solid), and 4% BHO only, and 4% BZO (BHO) plus 3% Y_2O_3 (open) doped YBCO nanocomposite films (a)-(b) 1.0 T (circle) and 3.0 T (triangle) at 77 K, (c)-(d) 5.0 T (circle), and 9.0 T (triangle) at 65 K respectively. Symbols for SD and DD follow the same for all figures.

film at 77 K and 65 K respectively is about three times higher than the $F_{p,max}$ ~7.4 GN/m^3 and 68 GN/m^3 value of 4% DD film at given temperature (Table I). Similarly, $F_{p,max}$ of BHO films are more than 2.0 times higher compared to their BZO counterparts at both temperatures of 77 K and 65 K. It means to compare the areal density of APCs concentration H_{max} (at which $F_{p,max}$ is observed), values are given in Table I, shows that not only higher number density of APCs are effectively active in vortex pinning in BHO films but also higher pinning efficiency (H_{max}/H^*) is observed in those films (Table I). In particular, $H_{max}/H^* \sim 1$ indicates the 100% pinning efficiency. At 77 K about 62% of the total APCs are effectively involved in vortex pinning in BHO SD film, which is about 50% higher, compared to its counterparts of BZO SD film when field is parallel to c-axis. At 65 K, it reaches to about 74% but it is still~ 10% less than BZO DD film. The higher H_{max}/H^* ~82% in BZO DD film could be due to mixed morphology of the APCs.

Figures 5(a)-(d) compare the pinning efficiency through H_{max}/H^* and $F_{p,max}$ with respect to θ dependence curves for the 4 vol.% BZO (BHO) SD and DD nanocomposite films. Figures 4(a)-(b) show that the general trend of the pinning efficiency is a downward trend as θ moves away from *H//c* and followed by an upward trend as the orientation moves closer to *H//ab*. The exception is the BZO DD sample which shows a slight peak at *H//ab* but a roughly flat trend from 0° to 67°. The $F_{p,max}$ values at *H//c* (Figures 5(c)-5(d)) show that the SD samples offer the strongest *c*-axis aligned APCs' pinning force over the DD samples. The $F_{p,max}$ of BHO SD is almost double (more than double) that of BZO SD at 77 K (65 K). Also, BHO DD pinning force is superior to that of BZO DD at both temperatures. This relatively outstanding strong pinning in the BHO samples could be attributed to their coherent APC/YBCO interface. Using an 80% threshold $F_{p,max}$ ratio the data (Figure 5(c)-(d)) suggest that the benefits of correlated pinning at both temperature extends up to ~ 22° in the BZO SD but falls short in the BZO DD sample. However, if we lower the criterion to 75%, then at 65 K both samples can be said to have the angular range of pinning extend to ~ 22°. As expected, reduced T_c effect also enhanced the pinning efficiency (H_{max}/H^*) as seen in Figure 5(a)-5(b). In addition, at 65 K the pinning efficiency at 22° is comparable to (in the case of BZO SD) or greater than (in the case of BZO DD) the pinning efficiency at 0°. One possibility is that at 22° and 65 K more APCs become active and or a situation where we have more than one pinned vortex per APC on average [20].

Figures 6(a)-(b) and 6c-d compare the $J_c(\theta)$ curves for the BZO (BHO) SD and DD nanocomposite films of 4 vol.% BHO concentrations at 77 K and 1.0 T and 3.0 T, and 65 K and at 5.0 T and 9.0 T respectively. As expected (due to the presence of mixed APCs), the DD nanocomposite films show a lower $J_c(\theta)$ anisotropy than the SD nanocomposite films. At 77 K the BZO SD (DD) films outperforms their BHO SD (DD) counterparts. When the temperature is lowered to 65 K the trend is reversed with the BHO SD (DD) samples having a lower anisotropy than the BZO SD (DD) films (except at 9 T where the BZO DD and BHO DD share the same anisotropy). This suggests that, at 77 K, the BHO samples (due to their relatively lower T_c values) are more susceptible to T_c effect than their BZO counterparts.

IV. Conclusion

This work investigates the pinning efficiency of BZO or BHO 1D APCs in two sets of samples: the single-doped 4 vol.% BZO and BHO/YBCO nanocomposites and double-doped 4 vol.% BZO (BHO) +3vol.% 3D Y_2O_3/YBCO nanocomposite thin films. In all samples, BZO or BHO 1D APCs of comparable diameter of 5-6 nm are formed along the *c*-axis providing strong correlated pinning at *H//c*-axis. However, the pinning efficiency

of these 1D APCs differs dramatically due to difference in the 1D APC/YBCO interfaces. In the single-doped samples, a coherent BHO/YBCO interface has been observed, which is in contrast to the semi-coherent BZO/YBCO interface due to a much higher concentration of defects such as dislocations. The difference in the 1D APC/YBCO interface has been found to have a profound effect on the pinning efficiency of the 1D APCs and higher pinning efficiency has been observed on BHO 1D APC/YBCO. At 77 K, the $F_{p,max} \sim 122.8$ GN/m^3 in BHO SD film compared to $F_{p,max} \sim 13.3$ GN/m^3 for BZO SD films. At 65 K, the $F_{p,max} \sim 182$ GN/m^3 in BHO SD film is about 2.5 times higher than that of its BZO SD counterpart. In addition, the $H_{max}/H^* \sim 0.62$ and 0.74 for BHO SD film is about 1.5 times higher than that of the $H_{max}/H^* \sim 0.43$ and 0.53 of BZO SD film at 77 K and 65 K respectively. In double doped films, the addition of Y_2O_3 could make a difference on morphology of the 1D APCs that might affect the H_{max}/H^* values. At 77 K, the H_{max}/H^* is about 0.6 for BZO DD compared to $H_{max}/H^* \sim 0.32$ for BHO DD films while at 65 K, H_{max}/H^* ratio reaches to 0.82 for former which is higher than the $H_{max}/H^* \sim 0.65$ for latter ones. This could be due to higher rigidity of BZO to form c-axis aligned 1D APCs even with the presence of secondary doping of Y_2O_3 compared to less rigidity of BHO. In addition, an extension of pinning efficiency of 1D APCs in BZO nanocomposite films at an angular range of 22° is observed. However, the extension of efficient pinning in BZO DD films could be explained as the presence of Y_2O_3 3D APCs and or more than one pinned vortices per one 1D APCs.

REFERENCES

[1] S. Foltyn *et al.*, "Materials science challenges for high-temperature superconducting wire," in *Materials For Sustainable Energy: A Collection of Peer-Reviewed Research and Review Articles from Nature Publishing Group*. Singapore: World Scientific, 2011, pp. 299–310.

[2] X. Obradors and T. Puig, "Coated conductors for power applications: materials challenges," *Supercond. Sci. Technol.*, vol. 27, no. 4, 2014, Art. no. 044003.

[3] S. Chen *et al.*, "Generating mixed morphology $BaZrO_3$ artificial pinning centers for strong and isotropic pinning in $BaZrO_3$–Y_2O_3 double-doped YBCO thin films," *Supercond. Sci. Technol.*, vol. 30, no. 12, 2017, Art. no. 125011.

[4] S. A. Harrington, J. H. Durrell, and B. Maiorov, "Self-assembled, rare earth tantalate pyrochlore nanoparticles for superior flux pinning in $YBa_2Cu_3O_{7-\delta}$ films," *Supercond. Sci. Technol.*, vol. 22, 2009, Art. no. 022001.

[5] K. Matsumoto and P. Mele, "Artificial pinning center technology to enhance vortex pinning in YBCO coated conductors," *Supercond. Sci. Technol.*, vol. 23, no. 1, 2009, Art. no. 014001.

[6] P. Mele *et al.*, "Systematic study of $BaSnO_3$ doped $YBa_2Cu_3O_{7-x}$ films," *Phys. C*, vol. 469, nos. 15–20, pp. 1380–1383, 2009.

[7] S. H. Wee, Y. L. Zuev, C. Cantoni, and A. Goyal, "Engineering nanocolumnar defect configurations for optimized vortex pinning in high temperature superconducting nanocomposite wires," *Sci. Rep.*, vol. 3, 2013, Art. no. 2310.

[8] J. Gutierrez *et al.*, "Strong isotropic flux pinning in solution-derived $YBa_2Cu_3O_{7-x}$ nanocomposite superconductor films," *Nature Mater.*, vol. 6, no. 5, pp. 367–373, 2007.

[9] V. Selvamanickam, M. H. Gharahcheshmeh, A. Xu, E. Galstyan, L. Delgado, and C. Cantoni, "High critical currents in heavily doped (Gd, Y) Ba_2Cu_3Ox superconductor tapes," *Appl. Phys. Lett.*, vol. 106, no. 3, 2015, Art. no. 032601.

[10] B. Maiorov *et al.*, "Synergetic combination of different types of defect to optimize pinning landscape using $BaZrO_3$-doped $YBa_2Cu_3O_7$," *Nature Mater.*, vol. 8, no. 5, pp. 398–404, 2009.

[11] C. V. Varanasi *et al.*, "Flux pinning enhancement in $YBa_2Cu_3O_{7-x}$ films with $BaSnO_3$ nanoparticles," *Supercond. Sci. Technol.*, vol. 19, no. 10, 2006, Art. no. L37.

[12] D. Larbalestier, A. Gurevich, D. M. Feldmann, and A. Polyanskii, "High-tc superconducting materials for electric power applications," *Nature*, vol. 414, no. 6861, pp. 368–377, 2001.

[13] E. Talantsev *et al.*, "Oxygen deficiency, stacking faults and calcium substitution in MOD YBCO coated conductors," *IEEE Trans. Appl. Supercond.*, vol. 23, no. 3, Jun. 2013, Art. no. 7200205.

[14] X. Obradors *et al.*, "Epitaxial $YBa_2Cu_3O_{7-x}$ nanocomposite films and coated conductors from $BaMO_3$ (M = Zr, Hf) colloidal solutions," *Supercond. Sci. Technol.*, vol. 31, no. 4, 2018, Art. no. 044001.

[15] B. Gautam *et al.*, "Microscopic adaptation of $BaHfO_3$ and Y_2O_3 artificial pinning centers for strong and isotropic pinning landscape in $YBa_2Cu_3O_{7-x}$ thin films," *Supercond. Sci. Technol.*, vol. 31, no. 2, 2018, Art. no. 025008.

[16] J. Mac Manus-Driscoll *et al.*, "Strongly enhanced current densities in superconducting coated conductors of $YBa_2Cu_3O_{7-x} + BaZrO_3$," *Nature Mater.*, vol. 3, pp. 439–443, 2004.

[17] B. Gautam *et al.*, "Transformational dynamics of BZO and BHO nanorods imposed by Y_2O_3 nanoparticles for improved isotropic pinning in $YBa_2Cu_3O_{7-\delta}$ thin films," *AIP Adv.*, vol. 7, no. 7, 2017, Art. no. 075308.

[18] S. Miura *et al.*, "Flux pinning properties in $BaHfO_3$-doped $SmBa_2Cu_3O_y$ films on metallic substrates fabricated with low temperature growth," *IEEE Trans. Appl. Supercond.*, vol. 26, no. 4, Jun. 2016, Art. no. 8000105.

[19] C. Cantoni *et al.*, "Strain-driven oxygen deficiency in self-assembled, nanostructured, composite oxide films," *ACS Nano*, vol. 5, no. 6, pp. 4783–4789, 2011.

[20] A. K. Jha *et al.*, "Tailoring the vortex pinning strength of YBCO thin films by systematic incorporation of hybrid artificial pinning centers," *Supercond. Sci. Technol.*, vol. 28, no. 11, 2015, Art. no. 114004.